GDCh

Communications

Angewandte
Chemie
International Edition
www.angewandte.org

VIP | Water Splitting | *Very Important Paper*

Coordination Chemistry Engineered Polymeric Carbon Nitride Photoanode with Ultralow Onset Potential for Water Splitting

Xiangqian Fan, Zhiliang Wang,* Tongen Lin, Du Du, Mu Xiao, Peng Chen,
Sabiha Akter Monny, Hengming Huang, Miaoqiang Lyu, Mingyuan Lu, and
Lianzhou Wang*

Abstract: Construction of an intimate film/substrate interface is of great importance for a photoelectrode to achieve efficient photoelectrochemical performance. Inspired by coordination chemistry, a polymeric carbon nitride (PCN) film is intimately grown on a Ti-coated substrate by an in situ thermal condensation process. The as-prepared PCN photoanode exhibits a record low onset potential (E_{onset}) of -0.38 V versus the reversible hydrogen electrode (RHE) and a decent photocurrent density of 242 $\mu A\,cm^{-2}$ at 1.23 V_{RHE} for water splitting. Detailed characterization confirms that the origin of the ultralow onset potential is mainly attributed to the substantially reduced interfacial resistance between the Ti-coated substrate and the PCN film benefitting from the constructed interfacial sp^2 N→Ti coordination bonds. For the first time, the ultralow onset potential enables the PCN photoanode to drive water splitting without external bias with a stable photocurrent density of $\approx 9\,\mu A\,cm^{-2}$ up to 1 hour.

As an abundant and renewable energy source, solar energy is among the best candidates to resolve the challenges of

fossil fuel shortage and climate change.[1] Directly converting solar energy into green hydrogen by photoelectrochemical (PEC) water splitting is considered to be a promising strategy in terms of energy storage and transportation.[2] As a metal-free semiconductor, polymeric carbon nitride (PCN) has attracted much attention in the photocatalysis field during the past decade due to its merits of suitable electronic band structure, facile preparation/modification and high chemical stability.[3] Despite enormous work dealing with photocatalytic properties of PCN powder, implementation of PCN-based photoelectrodes for photoelectrochemical (PEC) water splitting is still at its infancy. The current research is mainly focused on developing reliable film growth strategies to obtain high-performance PCN photoelectrodes.[4]

Generally, PCN photoanodes fabricated from well-prepared PCN powder only bear weak Van de Waals bonds between PCN particles and substrates, which seriously limits the charge transfer and results in poor PEC performance in terms of both photocurrent density (normally several $\mu A\,cm^{-2}$) and onset potential.[5–7] Recently, various in situ techniques such as thermal vapor condensation,[8] template-confined condensation,[9] seed crystallization–condensation[10] and microwave-assisted condensation,[11] etc. have been developed in order to obtain compact PCN films on conductive substrates. The photocurrent density of these PCN photoelectrodes has seen an increase up to 50–350 $\mu A\,cm^{-2}$ at 1.23 V_{RHE}, whereas the onset potential (E_{onset}) remained above 0 V_{RHE} in most cases (Table S1). According to Gartner's equation, the theoretical E_{onset} is close to the flat band potential.[12] Given the very negative conduction band (up to -1.3 V_{RHE}) of PCN,[13] there is much room for further lowering the E_{onset}, yet there is very limited progress to date.

For a given semiconductor-based photoanode with a certain electronic band structure, the E_{onset} is solely dependent on the overpotential in PEC process,[14] which includes ohmic, kinetic, and mass transfer overpotentials.[15] Reducing the ohmic overpotential (i.e. total cell internal resistance including electronic, interface, and ionic resistance[16]) is of great significance to improve the PEC water splitting performance as it concerns the expedite transport of charge carriers and protons. Construction of a bulk semiconductor film with intimate contact with the substrate is crucial to reduce the overall resistance for the polymer-based photoelectrodes considering the low conductivity among polymer

[*] X. Fan, Dr. Z. Wang, T. Lin, Dr. M. Xiao, Dr. P. Chen,
Dr. S. A. Monny, Dr. M. Lyu, Dr. M. Lu, Prof. L. Wang
Nanomaterials Centre, School of Chemical Engineering and
Australian Institute for Bioengineering and Nanotechnology,
The University of Queensland
St Lucia, QLD 4072 (Australia)
E-mail: zhiliang.wang@uq.edu.au
l.wang@uq.edu.au

D. Du
School of Mechanical and Mining Engineering,
The University of Queensland
St Lucia, QLD 4072 (Australia)

Dr. H. Huang
State Key Laboratory of Materials-Oriented Chemical Engineering,
College of Materials Science and Engineering,
Nanjing Tech University
Nanjing 211816 (P.R. China)

aggregates in the bulk film. Regrettably, previous in situ PCN growth strategies mainly aimed to adjust the bulk film quality, whereas the film/substrate interface engineering has rarely been emphasized.

Considering there are abundant lone pair electrons on the sp2 nitrogen (−N=C−) in heptazine rings connected PCN, we were inspired by the concept of coordination chemistry to introduce coordination bonds between PCN and suitable transition metals with empty orbitals in the process of PCN synthesis. Though this coordination interaction has frequently seen on transition metal doped PCN in powder-based catalysis,[17] the concept has rarely been used to construct PCN photoelectrode. Herein, we report a titanium (Ti)-induced growth method to introduce strong sp2 N→Ti coordination bonds between the PCN film and the Ti-coated fluorine-doped SnO_2 (FTO) substrate during a thermal condensation process. Ti metal is selected based on the high chemical stability, as well as the cost-effective merit over noble metals. A record low E_{onset} of −0.38 V_{RHE} and a high photocurrent density of 242 $\mu A\,cm^{-2}$ at 1.23 V_{RHE} in

0.5 M H_2SO_4 electrolyte are achieved on the PCN photoanode under 1 sun illumination (AM 1.5 G). Improved interfacial contact, and hence accelerated charge transfer have been unambiguously characterized. The ultralow negative onset potential indicates that the PCN photoanode can realize unbiased water splitting, which has been confirmed by a stable short circuit photocurrent density of 9 $\mu A\,cm^{-2}$ up to 1 hour under 1 sun illumination.

Figure 1a schematically shows the fabrication strategy of PCN photoelectrode on a Ti film (≈ 25 nm, the thickness was determined based on the comparison shown in Figure S1) coated FTO substrate from dicyandiamide precursor. The film thickness can be roughly tuned by changing the dicyandiamide amount. To obtain a good balance between light harvesting, bulk charge transfer and film coverage, 5 gram of dicyandiamide was applied in this study. During the temperature ramping process, dicyandiamide molecules melt (melting point: 209.5 °C) and disperse homogeneously on the FTO substrate, later annealing at 250 °C leads to a uniform precursor film. Eventually the
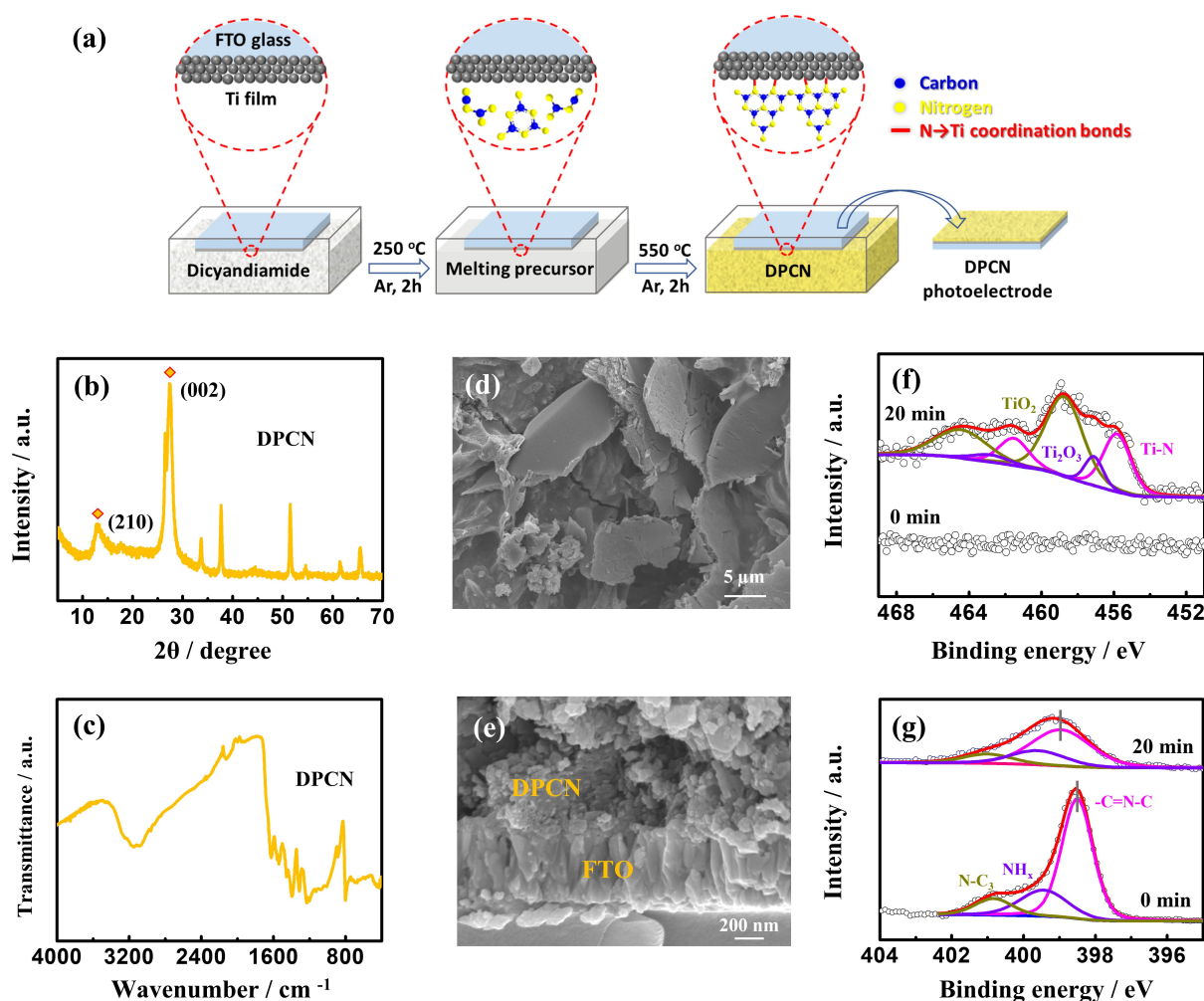

Figure 1. a) Schematic illustration of the procedure for Ti-induced growth of PCN film. b) XRD pattern of the DPCN photoelectrode. All other unlabeled peaks are assigned to FTO. c) FT-IR spectrum of the DPCN powder scratched from the DPCN photoelectrode. Top view (d) and regional cross-sectional (e) SEM images of the DPCN photoelectrode. f) Ti2p and g) N1s XPS core-level spectra of the DPCN photoelectrode after being ion-etched for 0 min and 20 min. The etching was conducted after mechanically removing the top thick film by blade.

precursor film converts to PCN film at 550 °C after a polycondensation process. The PCN featuring structure of the as-prepared photoelectrode is confirmed by the X-ray diffraction (XRD) pattern shown in Figure 1b. Specifically, the two peaks at 13.0° (210) and 27.5° (002) are ascribed to the in-plane structural motif and the interplanar stacking of heptazine-based layers of PCN, respectively.[18] In addition, the Fourier transform infrared (FT-IR) spectrum of the as-prepared photoelectrode (Figure 1c) also reveals the typical characteristic peaks belonged to PCN: the absorption bands at 1200–1700 cm^{-1} are ascribed to the stretching vibration modes of the heptazine units; the intense peak at 801 cm^{-1} originates from the out-of-plane bending vibration of the heptazine units; and the absorption bands at 2800–3400 cm^{-1} are attributed to the NH_x components and the O–H bands associated with adsorbed H_2O molecules.[19] Hereafter, we denote the as-prepared photoelectrode as DPCN (dicyandiamide-derived PCN). The DPCN photoelectrode has a band gap of ca. 2.80 eV (Figure S2b) estimated by UV/Vis diffuse reflectance spectroscopy (Figure S2a).

The morphology of the DPCN photoelectrode was investigated by scanning electron microscope (SEM). The top-view image and cross-sectional image (Figure 1d and e) show that the DPCN film features with small gaps, which allows for the diffusion of electrolytes and products despite the thick thickness (Figure S3). Figure 1e indicates the intimate contact between the DPCN film and the Ti-FTO substrate. To reveal the chemical bonds bridging the DPCN film and the Ti-FTO substrate, X-ray photoelectron spectroscopy (XPS) depth profile measurements were performed. Ti2p core level spectra (Figure 1f) verify the existence of Ti–O (Ti_2O_3, TiO_2)[20] and Ti–N[21] bonds on the DPCN/Ti-FTO interface (ion-etched for 20 min). The Ti–O (amorphous TiO_x) bonds are ascribed to the inevitably oxidation

of the surface Ti metal exposed in air (Figure S4).[22] The Ti–N bonds are supposed to originate from the coordination interaction between the Ti and the sp^2 nitrogen rather than TiN, since no N1s signal (Figure 1g) attributed to TiN (centered at ≈397.20 eV[23]) is observed. On the other hand, the sp^2 nitrogen (–C=N–C) peak (Figure 1g) on the top-surface (0 min) of the DPCN film is centered at 398.50 eV, whereas that of on the DPCN/Ti boundary (ion-etched for 20 min) locates at 398.96 eV: the apparent positive shift of the sp^2 nitrogen as a result of the electron donating from N to Ti further strengthen the evidence of the N→Ti coordination interaction on the DPCN/Ti interface.[24]

In order to rationally investigate the adhesive properties of the DPCN film on the Ti-FTO substrate, the nano-scratch tests[25] were carried out. The DPCN powder photoelectrode prepared by an electrophoretic method is presented for comparison. In nano-scratch testing (Figure 2a, testing sequence indicated by arrows), the nanoindenter vertically inserts the film under a vertically downward load, the scratching energy is then measured by laterally scratching the film (on the substrate), the nanoindenter goes back to the original position after unloading. Figure 2b and c show the scratches where the DPCN powder film has much clearer rim than the DPCN film, suggesting the latter one is much more firmly attached on the substrate. This result is quantitatively revealed by the scratch energy as shown in Figure 2d. It shows that scratching force of PCN is over 8 times higher than the PCN powder, which unambiguously demonstrates the effectiveness of forming intimate contact via the Ti-induced polymerization method.

Nyquist electrochemical impedance spectra (EIS) plots of the DPCN and the DPCN powder photoelectrodes are presented in Figure 3a and both can be fitted properly by a 2-RC-circuit model[26] (Figure S5a). The calculated parame-
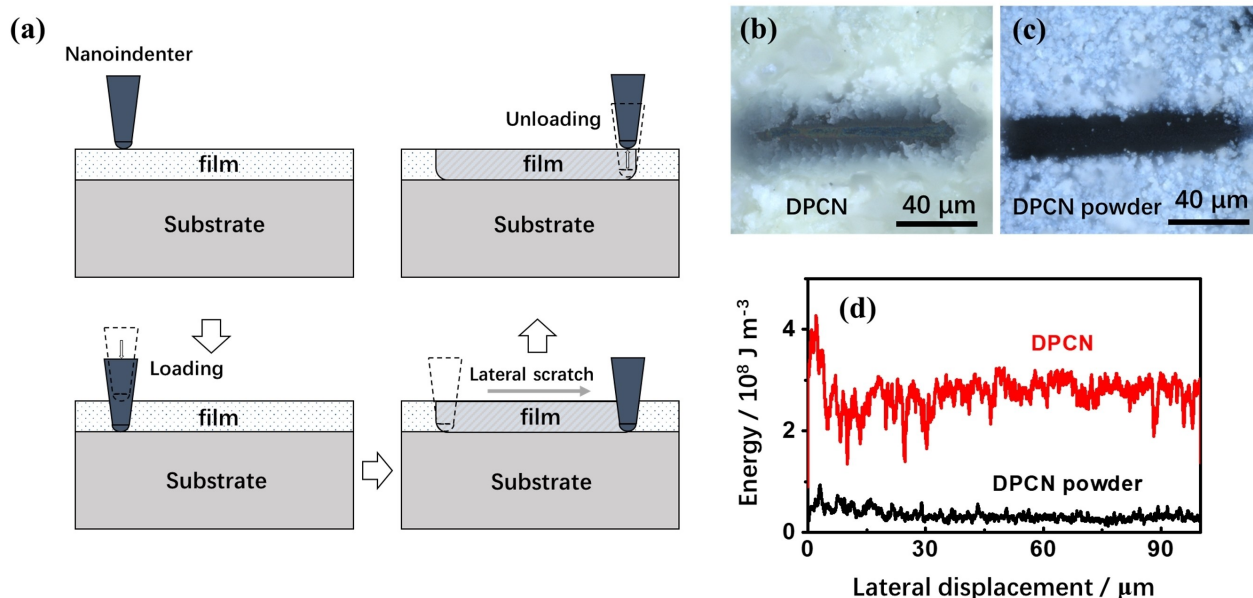

Figure 2. a) Schematic illustration of the nano-scratch process on DPCN film. Optical images of scratches made on the DPCN (b) and the DPCN powder (c) photoelectrodes. d) Scratching energies for the DPCN and the DPCN powder photoelectrodes varied with the lateral displacements.
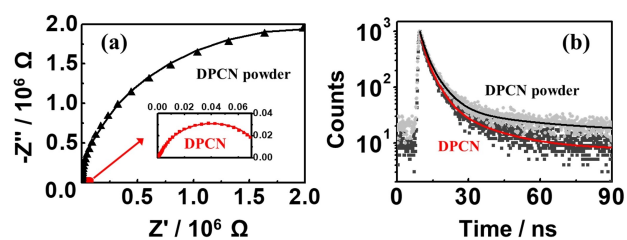
Figure 3. As-measured (dots) and fitted (lines) a) Nyquist plots of the DPCN and the DPCN powder photoelectrodes at 1.23 V_{RHE} under 1 sun illumination, and b) TRPL decay spectra of the DPCN and the DPCN powder photoelectrodes.
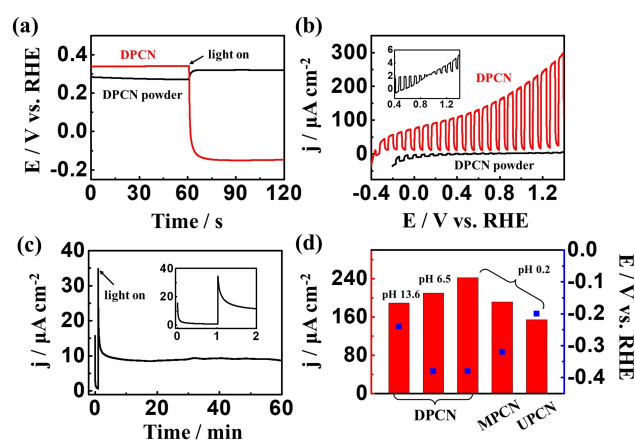

Figure 4. a) OCP measurements of the DPCN and the DPCN powder photoelectrodes in 0.5 M H_2SO_4 aqueous solution upon on/off one sun illumination. b) LSV curves of the DPCN and the DPCN powder photoelectrodes in 0.5 M H_2SO_4 aqueous solution under chopped 1 sun illumination. Inset is the chopped LSV curve of the DPCN powder photoelectrode in the range of 0.4–1.4 V_{RHE}. c) Zero bias photocurrent density of the DPCN photoelectrode in 0.5 M H_2SO_4 aqueous solution under continuous 1 sun illumination. d) Comparison of the photocurrent densities (red bar) and onset potentials (blue dot) of the DPCN photoelectrode in different electrolytes (0.5 M H_2SO_4, pH 0.2; 0.5 M Na_2SO_4, pH 6.5; 1 M NaOH, pH 13.6) and different precursors derived PCN (DPCN, MPCN, UPCN) in 0.5 M H_2SO_4 aqueous solution.

ters are shown in Figure S5b. Because of the strong coordination interaction, the observed bulk resistance of the DPCN photoelectrode (1.6 kOhm) is dramatically lower than that of the DPCN powder photoelectrode (21.6 kOhm). The charge transfer behavior between the DPCN film and the substrate is further disclosed by photoluminescence (PL) and Time-resolved photoluminescence (TRPL) measurements. The DPCN photoelectrode shows distinctly lower PL intensity than that of the DPCN powder photoelectrode (Figure S6a). Moreover, the TRPL spectra shown in Figure 3b indicate that DPCN photoelectrode also experienced a faster PL decay. Specifically, the average lifetime (Figure S6b) of the photogenerated charges in the DPCN photoelectrode is 7.26 ns, which is much shorter than that in the DPCN powder photoelectrode (12.77 ns). The lower PL intensity and shorter lifetime for the DPCN photoelectrode are attributed to the expedited charge transfer indebted from the strong interfacial coordination bonds directing the flow of the photogenerated electrons from the DPCN film to the Ti-FTO substrate.[8d]

The negative shift of the open circuit potential (OCP) (Figure 4a) of the DPCN photoelectrode from dark to light indicative of a typical n-type characteristic behavior, while the DPCN powder photoelectrodes exhibits a p-type feature according to the positive-shifted OCP, which is probably ascribed to the electron trap states in powder-based PCN photoelectrodes.[27] The difference between OCP_{dark} and OCP_{light} (ΔOCP) reflects the charge separation property of photoelectrodes.[28] We notice the ΔOCP of the DPCN photoelectrode is 10 times higher over that of the DPCN powder one (≈ 0.49 V vs. 0.05 V), indicating the favorable charge separation ability as proved previously. The enhanced charge separation of the DPCN photoelectrode exhibits its advantage for PEC water splitting in terms of both photocurrent density and onset potential as shown in the linear sweep voltammetry (LSV) curves in Figure 4b and Figure S7a. The underneath Ti-FTO substrate shows negligible photocurrent density ($\approx 10 \, \mu A \, cm^{-2}$) as displayed in Figure S7a inset. After depositing DPCN, the photoelectrode shows a photocurrent density of 242 $\mu A \, cm^{-2}$ at 1.23 V_{RHE} in 0.5 M H_2SO_4 solution (pH 0.2), which is two orders of magnitude higher than that of the DPCN powder photoelectrode. It should be noted that DPCN photoelectrode has an E_{onset} of $\approx -0.38 \, V_{RHE}$. To our knowledge,

this is the lowest onset potential among reported PCN photoanodes (Table S1), which is also superior to most of the metal-based photoanodes.[29] The flat band potential of DPCN photoelectrode is determined to be $-1.03 \, V_{RHE}$ revealed by the Mott–Schottky curve in Figure S7b. As stated before, the theoretical E_{onset} of a photoanode is close to the flat band potential, and the total overpotential (ohmic, kinetic, and mass transfer overpotential) determines the actual E_{onset}. Considering no water oxidation catalyst or additional passivation layer is attached on the DPCN film to lower the kinetic overpotential, and electrolyte with sufficient concentration already minimizes the mass transfer overpotential, the ultralow E_{onset} of the DPCN photoanode should be mainly attributed to the much reduced ohmic overpotential resulted from the decreased interfacial resistance. The reduced ohmic overpotential accelerates the surface reaction, which was evaluated by the hole extraction property determined by comparing the photocurrent density with and without a typical hole scavenger methanol (MeOH). As shown in Figure S7c, adding MeOH apparently improved the photocurrent density of the DPCN photoelectrode. If assuming the hole extraction efficiency is 100% with MeOH in the electrolyte, the hole extraction efficiency of the DPCN photoelectrode is estimated to be 75% at 1.23 V_{RHE} in 0.5 M H_2SO_4 without MeOH, which is impressive given the sluggish kinetics for metal-free PCN without water oxidation catalyst. As a comparison, the hole extraction efficiencies of state-of-art PCN photoanodes ranges from 50–73%.[10,11,30]

The ultralow onset potential below 0 V_{RHE} of the DPCN photoelectrode, as well as the negative value of the OCP_{light},

making it a potential candidate to realize PEC water splitting without an external bias.[31] Figure 4c confirms the availability to employ the DPCN photoelectrode for un-biased water splitting. It exhibits a stable photocurrent density of $\approx 9\,\mu A\,cm^{-2}$ over 60 min. The spike-like decrease at the beginning of dark- and photo-current (Figure 4c, inset) is attributed to the equilibrium process of the new double layer and the new space charge layer.[32] When extended the stability test to 6 h as shown in Figure S8 (black curve), the unbiased photocurrent gradually decreases. The activity decay is frequently observed on PCN photoanodes, which should be attributed to the self-photo-oxidation of PCN fragments by accumulated holes due to sluggish surface reaction,[10,33] similar to the case of inorganic nitrides.[34] The decomposition of PCN induces the breakage of the N→Ti coordination bonds, as attested by the interfacial Ti2p core level spectra of the DPCN photo-electrode after stability test (Figure S9). When MeOH scavenger was added into the electrolyte to eliminate the hole accumulation, the photocurrent density can be main-tained for a relatively long time (Figure S8, red curve), as photo-corrosion is inhibited. This result highlights the necessity of cocatalysts-deposition to suppress photo-corro-sion, since it can accelerate reaction kinetics to consume holes in time,[35] which will be our next step to improve the PEC performance of this PCN photoanode.

High photocurrent and low onset potential of the DPCN photoelectrode are observed over a wide pH range (pH 0.2–13.6) as shown in Figure 4d (see Figure S7d in detail). It affords a probability for its combination with various acid-nonresistant or base-nonresistant photocathodes to con-struct efficient bias-free overall water splitting PEC devices. Moreover, this Ti-induced PCN photoelectrodes could be achieved with various precursors, like melamine and urea. The morphology/thickness, and related composition charac-terizations (XRD/FT-IR) of MPCN (melamine-derived PCN) and UPCN (urea-derived PCN) photoelectrodes are displayed in Figure S10, indicating the generic feature of this film preparation method. Interestingly, the UPCN film has a nanotube structure, the detailed formation mechanism of the nanotubes is given in Figure S11. Both MPCN and UPCN exhibit a photocurrent density over $150\,\mu A\,cm^{-2}$ and an E_{onset} lower than $-0.2\,V_{RHE}$ (Figure 4d and Figure S12) in $0.5\,M\,H_2SO_4$ aqueous solution.

In summary, we have engineered the DPCN/substrate interface by constructing sp^2 N→Ti coordination bonds between the DPCN film and the Ti-FTO substrate, which has been verified by various characterizations. The DPCN photoelectrode thus exhibits conspicuous reduction of the interfacial electrical resistance compared with that of the powder photoelectrode counterpart, as revealed by the EIS, (TR)PL, and OCP measurements. The much improved charge transfer endows the DPCN photoanode with a record low onset potential of $\approx -0.38\,V_{RHE}$ and a high photocurrent density of $242\,\mu A\,cm^{-2}$ at $1.23\,V_{RHE}$ in $0.5\,M\,H_2SO_4$ aqueous solution under 1 sun illumination. Being indebted to the ultralow onset potential, the DPCN photoelectrode can drive un-biased PEC water splitting with a stable photo-current density $\approx 9\,\mu A\,cm^{-2}$ up to 1 hour. This Ti-induced

method to construct solid PCN/substrate interface is appli-cable to various PCN precursors. We believe the interfacial engineering strategy will inspire a way to solidly grow polymer semiconductors containing nitrogen/oxygen atoms with lone pair electrons on specific metal substrates for solar energy conversion application.

Conflict of Interest

The authors declare no conflict of interest.

Data Availability Statement

The data that support the findings of this study are available from the corresponding author upon reasonable request.

Keywords: Carbon Nitride · Coordination Bonds · Interfacial Engineering · Photoanode · Water Splitting

[1] N. Armaroli, V. Balzani, *Angew. Chem. Int. Ed.* **2007**, *46*, 52–66; *Angew. Chem.* **2007**, *119*, 52–67.

[2] a) M. G. Walter, E. L. Warren, J. R. McKone, S. W. Boettcher, Q. Mi, E. A. Santori, N. S. Lewis, *Chem. Rev.* **2010**, *110*, 6446–6473; b) C. Jiang, S. J. A. Moniz, A. Wang, T. Zhang, J. Tang, *Chem. Soc. Rev.* **2017**, *46*, 4645–4660.

[3] a) Y. Wang, X. Wang, M. Antonietti, *Angew. Chem. Int. Ed.* **2012**, *51*, 68–89; *Angew. Chem.* **2012**, *124*, 70–92; b) X. Wang, S. Blechert, M. Antonietti, *ACS Catal.* **2012**, *2*, 1596–1606; c) Y. Zheng, J. Liu, J. Liang, M. Jaroniec, S. Z. Qiao, *Energy Environ. Sci.* **2012**, *5*, 6717–6731; d) S. Cao, J. Low, J. Yu, M. Jaroniec, *Adv. Mater.* **2015**, *27*, 2150–2176; e) W.-J. Ong, L.-L. Tan, Y. H. Ng, S.-T. Yong, S.-P. Chai, *Chem. Rev.* **2016**, *116*, 7159–7329.

[4] M. Volokh, G. Peng, J. Barrio, M. Shalom, *Angew. Chem. Int. Ed.* **2019**, *58*, 6138–6151; *Angew. Chem.* **2019**, *131*, 6198–6211.

[5] Y. Zhang, M. Antonietti, *Chem. Asian J.* **2010**, *5*, 1307–1311.

[6] Y. Yang, Y. Guo, F. Liu, X. Yuan, Y. Guo, S. Zhang, W. Guo, M. Huo, *Appl. Catal. B* **2013**, *142–143*, 828–837.

[7] a) J. Xu, M. Shalom, *ACS Appl. Mater. Interfaces* **2016**, *8*, 13058–13063; b) X. Fan, L. Zhang, R. Cheng, M. Wang, M. Li, Y. Zhou, J. Shi, *ACS Catal.* **2015**, *5*, 5008–5015.

[8] a) J. Bian, Q. Li, C. Huang, J. Li, Y. Guo, M. Zaw, R.-Q. Zhang, *Nano Energy* **2015**, *15*, 353.–361; b) X. Lv, M. Cao, W. Shi, M. Wang, Y. Shen, *Carbon* **2017**, *117*, 343–350; c) W. Xiong, S. Chen, M. Huang, Z. Wang, Z. Lu, R. Q. Zhang, *ChemSusChem* **2018**, *11*, 2497–2501; d) Q. Jia, S. Zhang, Z. Gao, P. Yang, Q. Gu, *Catal. Sci. Technol.* **2019**, *9*, 425–435.

[9] B. Guo, L. Tian, W. Xie, A. Batool, G. Xie, Q. Xiang, S. U. Jan, R. Boddula, J. R. Gong, *Nano Lett.* **2018**, *18*, 5954–5960.

[10] a) G. Peng, J. Albero, H. Garcia, M. Shalom, *Angew. Chem. Int. Ed.* **2018**, *57*, 15807–15811; *Angew. Chem.* **2018**, *130*, 16033–16037; b) J. Qin, J. Barrio, G. Peng, J. Tzadikov, L. Abisdris, M. Volokh, M. Shalom, *Nat. Commun.* **2020**, *11*, 4701.

[11] T. Zhao, Q. Zhou, Y. Lv, D. Han, K. Wu, L. Zhao, Y. Shen, S. Liu, Y. Zhang, *Angew. Chem. Int. Ed.* **2020**, *59*, 1139–1143; *Angew. Chem.* **2020**, *132*, 1155–1159.

[12] A. Hankin, F. E. Bedoya-Lora, J. C. Alexander, A. Regoutz, G. H. Kelsall, *J. Mater. Chem. A* **2019**, 7, 26162–26176.

[13] X. Wang, K. Maeda, A. Thomas, K. Takanabe, G. Xin, J. M. Carlsson, K. Domen, M. Antonietti, *Nat. Mater.* **2009**, *8*, 76–80.

[14] B. Iandolo, H. Zhang, B. Wickman, I. Zorić, G. Conibeer, A. Hellman, *RSC Adv.* **2015**, *5*, 61021–61030.

[15] B. Chmielowiec, T. Fujimura, T. Otani, K. Aoyama, T. Nohira, T. Homma, Y. Fukunaka, A. Allanore, *J. Electrochem. Soc.* **2019**, *166*, E323–E329.

[16] F. Barbir in *PEM Fuel Cells*, 2nd ed. (Ed.: F. Barbir), Academic Press, Boston, **2013**, pp. 33–72.

[17] a) J. Feng, H. Gao, L. Zheng, Z. Chen, S. Zeng, C. Jiang, H. Dong, L. Liu, S. Zhang, X. Zhang, *Nat. Commun.* **2020**, *11*, 4341; b) Y. Zheng, Y. Jiao, Y. Zhu, Q. Cai, A. Vasileff, L. H. Li, Y. Han, Y. Chen, S.-Z. Qiao, *J. Am. Chem. Soc.* **2017**, *139*, 3336–3339; c) X. Zhao, C. Deng, D. Meng, H. Ji, C. Chen, W. Song, J. Zhao, *ACS Catal.* **2020**, *10*, 15178–15185; d) L.-S. Zhang, X.-H. Jiang, Z.-A. Zhong, L. Tian, Q. Sun, Y.-T. Cui, X. Lu, J.-P. Zou, S.-L. Luo, *Angew. Chem. Int. Ed.* **2021**, *60*, 21751–21755; *Angew. Chem.* **2021**, *133*, 21919–21923.

[18] a) E. Alwin, W. Nowicki, R. Wojcieszak, M. Zieliński, M. Pietrowski, *Dalton Trans.* **2020**, *49*, 12805–12813; b) F. Fina, S. K. Callear, G. M. Carins, J. T. S. Irvine, *Chem. Mater.* **2015**, *27*, 2612–2618.

[19] C. Huang, Y. Wen, J. Ma, D. Dong, Y. Shen, S. Liu, H. Ma, Y. Zhang, *Nat. Commun.* **2021**, *12*, 320.

[20] M. Hannula, H. Ali-Löytty, K. Lahtonen, E. Sarlin, J. Saari, M. Valden, *Chem. Mater.* **2018**, *30*, 1199–1208.

[21] S.-Z. Kure-Chu, H. Sakuyama, E.-i. Suzuki, H. Yashiro, K. Sasaki, H. Segawa, T. Hihara, *J. Electrochem. Soc.* **2018**, *165*, A477–A486.

[22] R. Shvab, E. Hryha, L. Nyborg, *Powder Metall.* **2017**, *60*, 42–48.

[23] B. J. Burrow, A. E. Morgan, R. C. Ellwanger, *J. Vac. Sci. Technol. A* **1986**, *4*, 2463–2469.

[24] a) R. Hao, G. Wang, H. Tang, L. Sun, C. Xu, D. Han, *Appl. Catal. B* **2016**, *187*, 47–58; b) Y. Tan, Z. Shu, J. Zhou, T. Li, W. Wang, Z. Zhao, *Appl. Catal. B* **2018**, *230*, 260–268.

[25] a) J. Tomastik, R. Ctvrtlik, *EPJ Web Conf.* **2013**, *48*, 27–30; b) T. Sumitomo, H. Huang, L. Zhou, *Int. J. Mach. Tools Manuf.* **2011**, *51*, 182–189.

[26] T. Lopes, L. Andrade, F. Le Formal, M. Gratzel, K. Sivula, A. Mendes, *Phys. Chem. Chem. Phys.* **2014**, *16*, 16515–16523.

[27] Q. Ruan, T. Miao, H. Wang, J. Tang, *J. Am. Chem. Soc.* **2020**, *142*, 2795–2802.

[28] a) F. F. Abdi, L. Han, A. H. M. Smets, M. Zeman, B. Dam, R. van de Krol, *Nat. Commun.* **2013**, *4*, 2195; b) J. W. Moir, E. V. Sackville, U. Hintermair, G. A. Ozin, *J. Phys. Chem. C* **2016**, *120*, 12999–13012; c) Y. Hu, Y. Wu, J. Feng, H. Huang, C. Zhang, Q. Qian, T. Fang, J. Xu, P. Wang, Z. Li, Z. Zou, *J. Mater. Chem. A* **2018**, *6*, 2568–2576.

[29] a) Y. He, T. Hamann, D. Wang, *Chem. Soc. Rev.* **2019**, *48*, 2182–2215; b) S. Wang, G. Liu, L. Wang, *Chem. Rev.* **2019**, *119*, 5192–5247; c) D. K. Lee, D. Lee, M. A. Lumley, K.-S. Choi, *Chem. Soc. Rev.* **2019**, *48*, 2126–2157.

[30] N. Karjule, J. Barrio, L. Xing, M. Volokh, M. Shalom, *Nano Lett.* **2020**, *20*, 4618–4624.

[31] a) I. E. Paulauskas, J. E. Katz, G. E. Jellison, N. S. Lewis, L. A. Boatner, G. M. Brown, *J. Electrochem. Soc.* **2009**, *156*, B580; b) A. Martinez-Garcia, H. B. Russell, W. Paxton, S. Ravipati, S. Calero-Barney, M. Menon, E. Richter, J. Young, T. Deutsch, M. K. Sunkara, *Adv. Energy Mater.* **2018**, *8*, 1703247.

[32] a) F. Le Formal, N. Tétreault, M. Cornuz, T. Moehl, M. Grätzel, K. Sivula, *Chem. Sci.* **2011**, *2*, 737–743; b) T. Higashi, Y. Sasaki, Y. Kawase, H. Nishiyama, M. Katayama, K. Takanabe, K. Domen, *Catalysts* **2021**, *11*, 584.

[33] X. Li, J. Wang, J. Xia, Y. Fang, Y. Hou, X. Fu, M. Shalom, X. Wang, *ChemSusChem* **2022**, *15*, e202200330.

[34] Y. He, J. E. Thorne, C. H. Wu, P. Ma, C. Du, Q. Dong, J. Guo, D. Wang, *Chem* **2016**, *1*, 640–655.

[35] a) Y. Fang, Y. Hou, X. Fu, X. Wang, *Chem. Rev.* **2022**, *122*, 4204–4256; b) N. Karjule, C. Singh, J. Barrio, J. Tzadikov, I. Liberman, M. Volokh, E. Palomares, I. Hod, M. Shalom, *Adv. Funct. Mater.* **2021**, *31*, 2101724.